

A search for pulsars in subdwarf B binary systems and discovery of giant-pulse emitting PSR J0533–4524

L. C. Oostrum^{1,2*}, J. van Leeuwen^{1,2}, Y. Maan¹, T. Coenen^{2,1}, C.H. Ishwara-Chandra³

¹*ASTRON, The Netherlands Institute for Radio Astronomy, Oude Hoogeveensedijk 4, 7991 PD, Dwingeloo, The Netherlands*

²*Anton Pannekoek Institute for Astronomy, University of Amsterdam, PO Box 94249, 1090 GE, Amsterdam, The Netherlands*

³*National Centre for Radio Astrophysics, TIFR, Post Bag 3, Pune University Campus, 411007 Pune, India*

Accepted 2020 January 13. Received 2020 January 13; in original form 2019 October 11

ABSTRACT

Binary millisecond pulsars (MSPs) provide several opportunities for research of fundamental physics. However, finding them can be challenging. Several subdwarf B (sdB) binary systems with possible neutron star companions have been identified, allowing us to perform a targeted search for MSPs within these systems. Six sdBs with companions in the neutron star mass range, as determined from their optical light curves, were observed with the Green Bank and Westerbork radio telescopes. The data were searched for periodic signals as well as single pulses. No radio pulsations from sdB systems were detected, down to an average sensitivity limit of 0.11 mJy. We did, however, discover a pulsar in the field of sdB HE0532–4503. Follow-up observations with the Giant Metrewave Radio Telescope showed that this pulsar, J0533–4524, is not spatially coincident with the sdB system. The pulsar has a relatively low magnetic field but still emits giant pulses. We place an upper limit of three to the number of radio pulsars in the six sdB systems. The non-detections may be explained by a combination of the MSP beaming fraction, luminosity, and a recycling fraction <0.5 . Alternatively, the assumption of co-rotation between the MSP and sdB may break down, which implies the systems are more edge-on than previously thought. This would shift the predicted companion masses into the white dwarf range. It would also explain the relative lack of edge-on sdB systems with massive companions.

Key words: subdwarfs – stars: neutron – pulsars: general – pulsars: individual: J0533–4524

1 INTRODUCTION

In binary systems, accretion may convert normal pulsars (PSRs) into fast-spinning, low magnetic field, millisecond pulsars (MSPs). Timing pulse arrivals from pulsars in such systems in order to extract their properties offers tests and insights in a number of fundamental physics areas. One can constrain neutron star masses and equations of state (Lattimer & Prakash 2001), study binary evolution, and strong field general relativity (if the pulsar is in orbit with a massive companion, e.g. Taylor & Weisberg 1989). Furthermore, gravitational radiation from distant supermassive black hole mergers can potentially be detected using pulsar timing arrays made up of stably rotating and emitting pulsars (Jaffe & Backer 2003).

Finding new MSPs in a blind, wide-field survey is a challenge. Blind surveys for radio pulsars have led to discoveries of numerous MSPs (e.g. Bates et al. 2015; Sanidas et al. 2019; Parent et al. 2019). Targeted searches allow for an increased sensitivity and a more efficient use of telescope time (see, for example, Camilo et al. 2015; Maan et al. 2018). As MSPs need a binary companion for their formation, selecting targets based on potential companions

identified at optical wavelengths promises to be efficient. Generally these companions are assumed to be white dwarfs (van Leeuwen et al. 2007; Agüeros et al. 2009), but MSP - subdwarf systems are also possible. In those systems, a sub-luminous B dwarf star (sdB) would have spun up the MSP.

Sub-luminous B dwarfs (sdBs) are thought to be light ($\sim 0.5M_{\odot}$), core helium-burning stars. In contrast to main-sequence core helium-burning stars, they have thin hydrogen envelopes (Heber 1986) and a peculiar composition that does not fit the usual MK classification scheme (Drilling et al. 2013). A large fraction of sdBs – up to 2/3 for some surveys (Maxted et al. 2001) – are in tight (hours to days) binaries, but not all are. Thus, while binary evolution must be important in the development of these stars, their exact formation is a matter of ongoing debate. The detection of an MSP companion would therefore not only advance research into compact objects; it could also help explain the formation of subdwarf stars. Among the ~ 6000 hot subdwarf stars known in our Galaxy, ~ 3500 are sdB stars (Geier et al. 2017). There may be several million sdB stars, although a significant fraction may have been missed so far due to selection effects (Han et al. 2003). Several channels of binary evolution could have been responsible for producing the observed sdB population: Stable Roche-Lobe overflow could lead

* E-mail: l.c.oostrum@uva.nl

to a longer-period binary with a main-sequence companion (Han et al. 2003; Chen et al. 2013). They might also be formed through the merger of two white dwarfs, resulting in an isolated sdB (Webbink 1984). Lastly, a common envelope channel could lead to an sdB with a massive compact companion (Geier et al. 2010). This channel involves a wide binary with a massive primary, that will go on to form a neutron star (NS) or black hole (BH), two phases of common envelope evolution and a short X-ray binary phase. A first common envelope phase starts soon after the primary reaches the red supergiant stage of its evolution and starts overflowing its Roche Lobe. During this first common envelope phase the binary tightens. The second phase of mass transfer starts when the secondary begins to overflow its Roche Lobe. If the primary, which by then has undergone a supernova, is a neutron star it will get recycled. The second common-envelope phase starts shortly thereafter, tightens the binary further and dissipates the envelope of the secondary. The secondary, which is now mostly stripped of its hydrogen envelope, continues its evolution as an sdB star. For a recent review on sdB stars see Heber (2016).

Based on population synthesis, Yungelson & Tutukov (2005) find that in 9 out of 10 observed sdB binaries, the companion is a white dwarf. In 1 out of 10 it is a main sequence star. For compact object companions, simulations by Nelemans (2010) show that 1 in 100 sdB binaries contains a neutron star, and 1 in 10,000 a black hole. Thus, of the known sdB stars, a few dozen are expected to orbit a neutron star; a handful may be in a binary with a black hole. So far, no such compact-object companion has been directly confirmed. Positively identifying a pulsar in a tight, hours to days, sdB binary would provide constraints on binary evolution leading to these systems (see e.g. Coenen et al. 2011). The unique formation mechanism of sdB stars potentially creates remarkable binary systems where the orbit may even be relativistic. This suggests MSPs found in such targeted binaries may help constrain theories of gravity (cf. Freire et al. 2012). Furthermore, the timing of such an MSP would inform us of the size of the projected neutron-star orbit and the neutron-star velocity. Combined with a canonical neutron-star mass and measurement of the sdB velocity, this would provide a derivation of the sdB mass. If the MSP timing stability allows for the determination of post-Keplerian parameters, as in e.g., van Leeuwen et al. (2015), one can deduce these parameters more precisely still, to about 1%.

Given sufficiently deep observations, non-detections of radio pulsations from these systems could mean the absence of a neutron star, but may also be explained by a pulsar that is either off (because, for example, it was insufficiently recycled), or beamed away from Earth. Non-detections in a large enough sample of sdB stars provide statistics on the sdB formation channels.

In Sect. 2 our target selection is described. Section 3 gives an overview of our observations and data reduction. We show the results on sdB systems and the discovery of a new pulsar in Sects. 4 and 5. In Sect. 6 we discuss our findings and in Sect. 7 we show our conclusions.

2 CANDIDATE SELECTION

Our targets were selected from a sample of sdB stars presented in Geier et al. (2010). Using multiple optical spectra spread over the orbit of the sdBs, they determine the radial velocity curves and hence constrain the mass function:

$$f_m = \frac{M_{\text{comp}}^3 \sin^3 i}{(M_{\text{comp}} + M_{\text{sdB}})^2} = \frac{PK^3}{2\pi G}, \quad (1)$$

where M_{sdB} and M_{comp} are the masses of the sdB and its companion, i is the inclination angle of the orbital plane, P is the orbital period, and K is the radial velocity semi-amplitude of the sdB.

Under the assumption that the sdBs are tidally locked, the inclination can be determined from their observed rotational velocities. Furthermore, in a binary, the sdB mass resulting from the common-envelope ejection channel is predicted to be in a very narrow range of 0.46 - 0.50 M_{\odot} , with a canonical value of 0.46 M_{\odot} (Han et al. 2002, 2003). However, in those cases the companion is typically a white dwarf. For neutron star companions, the allowed mass range may be larger, 0.3-1.1 M_{\odot} (Geier et al. 2010). For the systems discussed in this paper, Geier et al. (2010) could not determine the sdB mass but used a canonical value of 0.5 M_{\odot} . The derived inclinations then led to predictions for the companion masses (Geier et al. 2010).

Out of the 31 systems for which an estimate for the companion mass was determined, six have companions whose derived mass is above the Chandrasekhar limit, hence these are considered candidate neutron stars. Four of these are at least 1σ above the Chandrasekhar limit. The common envelope channel predicted to lead to such sdB binary systems with a massive compact companion also suggests mass transfer onto the compact object (Geier et al. 2010). As this is the canonical scenario for creating an MSP (Radhakrishnan & Srinivasan 1982; Alpar et al. 1982), the neutron star candidates are considered to be MSP candidates as well. As the masses are the only argument for the companions being neutron stars, some of them might, however, be white dwarfs (WDs).

Three of the candidates, HE 0929–0424, HE 0532–4503, and PG 1232–136, were already observed and analysed in Coenen et al. (2011). No pulsations were found there, and the pseudo-luminosity of any recycled pulsar in HE 0929–0424 and PG 1232–136 was strongly constrained. A weaker constrain was put on HE 0532–4503. Here we present an analysis of deeper observations of the same sources, as well as of three additional sources: PG 1101+249, PG 1432+159, and PG 1743+477. While PG 1232–136 is expected to host a black hole as its derived companion mass is a lower limit of 6 M_{\odot} (Geier et al. 2010), it might host a massive neutron star if the sdB in the binary system is not tidally locked. An overview of the targets is given in Table 1.

3 OBSERVATIONS AND DATA REDUCTION

The six targets were observed with either the Westerbork Synthesis Radio Telescope (WSRT) at 310-375 MHz, or the Robert C. Byrd Green Bank Telescope (GBT) at 300-400 MHz as shown in Table 1. WSRT is a tied array of 14 25-m dishes spread over a 3-km baseline, resulting in a beam size of 1' at 350 MHz. At the same frequency, the 100-m GBT has a beam size of 35'. For each target, the observation duration was chosen such that we would have detected 95-100% of the known MSPs when placed at the source distance (i.e., close to full completeness, see Coenen et al. 2011). In each observing session, a bright pulsar was observed as a test source to ensure that our observing setup and data reduction pipeline performed as expected.

The follow-up observations of a strong candidate from our search were performed using the GBT as well as the upgraded Giant Metrewave Radio Telescope (uGMRT; Gupta et al. 2017), and these are discussed in more detail in Sect. 5.

All data were searched with the PRESTO¹ package (Ransom

¹ <https://github.com/scottransom/presto>

Table 1. Overview of target parameters (based on Geier et al. 2010, distances from Gaia Data Release 2; Gaia Collaboration et al. 2018) and observations. GBT observations were carried out with GUPPI at 300–400 MHz, for WSRT we used PUMAR1 at 310–375 MHz. S_{\min} is the minimum detectable flux density for the full observation duration.

Target	l (°)	b (°)	P_{orb} (d)	i (°)	M_{comp} (M_{\odot})	Companion	Distance (kpc)	Telescope	MJD	t_{obs} (hr)	S_{\min} (mJy)
HE 0929–0424	238.52	+32.36	0.44	23^{+5}_{-4}	$1.82^{+0.88}_{-0.64}$	WD/NS/BH	1.7(3)	GBT	55687.03, 55690.91 ^(a)	0.5 + 0.8	0.11 ^(b)
HE 0532–4503	251.02	–32.14	0.27	14^{+2}_{-2}	$3.00^{+0.94}_{-0.92}$	NS/BH	2.9(5)	GBT	55852.34	2.1	0.07
PG 1101+249	212.76	+65.88	0.35	26^{+6}_{-4}	$1.67^{+0.77}_{-0.58}$	WD/NS/BH	0.43(1)	GBT	55715.00	2.0	0.07
PG 1232–136	296.99	+48.77	0.36	<14	>6.00	BH	0.50(1)	GBT	55687.08	0.9	0.12
PG 1432+159	012.83	+63.32	0.22	16^{+5}_{-3}	$2.59^{+2.01}_{-1.10}$	NS/BH	0.63(3)	WSRT	55634.89	3.8	0.22
PG 1743+477	074.41	+30.66	0.52	<27	> 1.66	NS/BH	0.77(2)	WSRT	55650.27	3.8	0.21

^(a) This source was observed in two separate sessions.

^(b) For the longest observation of this source.

2011). We used `RFIFIND` to create radio frequency interference (RFI) masks which were used with subsequent processing. For uGMRT data, any strong *periodic* RFI (such as 50 Hz interference from the power lines) were identified and excised from the individual frequency channels using `RFICLEAN`² (Maan & van Leeuwen in prep.).

Using the NE2001 (Cordes & Lazio 2002) and YMW16 (Yao et al. 2017) Galactic electron density models, we converted the sdB distances to an expected dispersion measure (DM) towards each source. Based on this, we chose a DM upper limit in our search of 500 pc cm^{-3} , which is well above the expected value of $\sim 50 \text{ pc cm}^{-3}$ predicted by the models. A higher value was chosen to account for the factor few uncertainty in Galactic electron density models, as well as uncertainties in the distance to the sources. Using `DDPLAN.PY` from PRESTO, a dedispersion plan was determined for each observation, taking into account the different time resolution and channel width for each instrument and optimised for minimal computing time at maximum resolution and sensitivity. This led to typically 10000 timeseries over a DM range of 0–500 pc cm^{-3} , with DM steps of 0.01 pc cm^{-3} for DMs $< 35 \text{ pc cm}^{-3}$ up to 0.3 pc cm^{-3} for DMs $> 400 \text{ pc cm}^{-3}$. Each resulting timeseries was searched for both single pulses and periodic signals, as described hereafter.

3.1 Periodicity search

The periodicity search was done in the frequency domain, using `ACCELSEARCH` from PRESTO. We searched for spin periods between 0.1 ms and 1 s. Up to 16 harmonics were summed to improve sensitivity to narrow pulses. The likely strong acceleration of the targets in their binary orbits causes a drift of the signal in Fourier space. This drift can be searched for by `ACCELSEARCH`, but only in the regime of constant acceleration. That assumption is typically valid if the observation is shorter than 10% of the orbital period. Most of our observations are, however, longer. For those, we searched both the full data, as well as chunks of at most 10% of the orbit.

The maximum expected line-of-sight acceleration (a_{max}) is given by

$$a_{\text{max}} = \Omega_b r_p = \left[\frac{GM_{\text{sdb}}^3 \Omega_b^4}{(M_{\text{sdb}} + M_p)^2} \right]^{1/3}, \quad (2)$$

² <https://github.com/ymaan4/rfiClean>

where Ω_b and r_p are the mean angular velocity and semi-major axis of the pulsar orbit, M_{sdb} and M_p are the masses of the sdB and pulsar, and G is the gravitational constant. The second equality is given by Kepler’s 3rd law, which is valid given the observed non-relativistic orbital velocities of the sdBs. The suspected neutron star companions are all more massive than the sdBs and hence have a lower orbital velocity. For a canonical pulsar of mass $1.4 M_{\odot}$ and sdB of mass $0.46 M_{\odot}$, the maximum acceleration ranges from 11 m s^{-2} for PG 1743+477 to 35 m s^{-2} for PG 1432+159. We use these values to set the maximum Fourier space drift in `ACCELSEARCH`, which then searches for accelerations between zero and the given value.

The candidates produced by `ACCELSEARCH` are sifted using `ACCEL_SIFT.PY` from PRESTO and each candidate with a signal-to-noise ratio (S/N) of 8 was folded on the raw data and visually inspected.

3.2 Single pulse search

Each timeseries was searched for single pulses using `SINGLE_PULSE_SEARCH.PY` from PRESTO. The S/N at each point in the timeseries is determined using a Fourier-domain matched-filter technique, with boxcar widths between one sample and the number of samples corresponding to 20 ms. This means the search is sensitive to single pulses with widths up to 20 ms. The matched-filtering is not sensitive to the phase of the pulse. All single-pulse candidates above a S/N of 8 were visually inspected.

4 RESULTS

All test pulsars were successfully detected by our pipeline. The single pulse search yielded similar results. The only test pulsar known to emit giant pulses, PSR B1937+21 (Cognard et al. 1996), was blindly re-detected. In our sample of six sdB systems, one pulsar candidate is identified towards sdB HE0532–4503 with a period of 157.28 ms and DM of 19 pc cm^{-3} (Fig. 1). In addition, three single pulses were detected towards HE 0532–4503 (Fig. 2). These were detected at the same DM as the periodic candidate.

The system was observed several times with GBT, Parkes and uGMRT (Table 2). Periodic emission from the pulsar was not detected in the first three follow-up observations on 20160528 to 20160530. Single pulses continued to be visible. From timing on these single pulses, and later on periodic detections, we learned the

pulsar was isolated and was found by chance in the sdB star field. The discovery of this pulsar, PSR J0533–4524, is further discussed in Sect. 5.

We thus detect no pulsars in any of the observed sdB binary systems. This does not directly imply none of these sdB systems host a pulsar. They could be too faint, or their emission could be beamed away from Earth.

An upper limit to the flux density of any pulsar beamed towards Earth can be set using the radiometer equation (Dewey et al. 1985; Lorimer & Kramer 2005):

$$S_{\min} = \frac{(S/N)_{\min} T_{\text{sys}}}{G \sqrt{N_{\text{pol}} BW T_{\text{obs}}}} \sqrt{\frac{W}{P - W}} \quad (3)$$

Where S_{\min} is the minimum detectable flux density, $(S/N)_{\min}$ is the S/N threshold in the search, T_{sys} is the sum of the receiver temperature (T_{rec}) and the sky temperature (T_{sky}), G is the telescope gain, N_{pol} is the number of polarisations ($=2$), BW is the bandwidth, T_{obs} is the length of the observation, P is the pulsar period and W is width of the pulse profile. As the putative pulsars are expected to be MSPs (here defined, following Manchester 2017, as pulsars with $P < 100$ ms and with $\dot{P} < 10^{-17}$), we adopt the median value of $W/P = 0.08$ of MSPs in the ATNF pulsar catalogue (Hobbs & Manchester 2004), where width is defined as the width at 50% of the maximum of the pulse profile. While this duty cycle is somewhat larger at lower frequencies – suggesting the beam illuminates a larger part of the celestial sphere over the pulsar, and increasing the odds of Earth being in it – the difference is negligible compared to the other uncertainties in determining S_{\min} . The sky temperature is taken from the Haslam et al. (1982) sky map, scaled from 400 MHz to the central frequency of each instrument using a scaling of $T_{\text{sky}} \propto \nu^{-2.6}$ (Lawson et al. 1987). For GBT we use $T_{\text{rec}} = 58$ K and $G = 2.0$ K/Jy³, for WSRT $T_{\text{rec}} = 125$ K and $G = 1.1$ K/Jy (Rubio-Herrera et al. 2013). The obtained flux density limits are listed in Table 1.

We run a Monte-Carlo (MC) simulation to determine how many pulsars we expect to detect. We use a pseudo-luminosity distribution following a log-normal distribution with mean -1.1 and standard deviation -0.9 (Faucher-Giguère & Kaspi 2006). This distribution was determined for normal pulsars at 1400 MHz, but later shown to be valid for recycled pulsars in globular clusters (Bagchi et al. 2011). The distribution is scaled from 1400 MHz to 350 MHz using a spectral index of -1.9 , which is a typical value as used in Bagchi et al. (2011).

The luminosity distribution gives the probability that a pulsar is bright enough to be detected from Earth, but ignores any beaming effect. The beams of MSPs are larger than those of normal pulsars, and their beaming fractions f_b are typically as high as 0.5 to 0.9 (Kramer et al. 1998). Still these do not cover the entire sky so there is a 10-50% chance the beam misses Earth. In our simulation, we assume a uniform distribution of f_b between 0.5 and 0.9.

For the MC simulation, we first assign N out of the six systems to actually host a pulsar. For each value of N from zero to six, we simulate $N \times 25000$ pulsars. Each pulsar is randomly assigned to one of the sdB systems, from which then a distance is drawn using a normal distribution with mean and standard deviation equal to the values determined for the sdB by Gaia (Gaia Collaboration et al. 2018, see also Table 1). The pulsar is also assigned a pseudo-luminosity and beaming fraction following the above described distributions. The pulsar is considered detected if (i) the flux density determined from

the pseudo-luminosity and sdB distance is above the threshold for the corresponding observation (see Table 1) and (ii) the pulsar beam sweeps across Earth, which is true with a probability equal to the beaming fraction.

When using the flux density threshold as determined for the full observation duration (cf. Table 1), we find that if more than three systems host a pulsar, we would have detected at least one in $>97\%$ of the iterations. As we also searched the data in chunks of at most 10% of the orbital duration of the sdBs to avoid strong acceleration effects, we repeat the simulation with flux density thresholds determined from the duration of those chunks. Then, we would have detected at least one pulsar in $>95\%$ of the iterations. We thus conclude that *at most* three of the sdB systems host an MSP. If they do host MSPs, these must either be very faint or their beam does not sweep across the Earth.

If pulsars in sdB systems are only mildly recycled, their beams may be larger. The beaming fraction is also the most important factor in the number of detectable pulsars; for a uniform beaming fraction distribution of 0.3-0.5, it is possible that all six systems host a pulsar at the 95% confidence level.

5 DISCOVERY OF PSR J0533–4524

One convincing pulsar candidate was detected in our data, towards sdB HE0532–4503. The candidate was detected with a S/N of 22 at a period of 157.28 ms and a DM of 19 pc cm^{-3} . The periodic pulse profile is shown in Fig. 1. The signal is broadband and clearly visible throughout most of the observation. In addition to the periodic signal, three single pulses were detected with a S/N between 10 and 30, all of which reached a maximum S/N at the DM of the periodic candidate. The brightest detected pulse is shown in Fig. 2.

The visible sdB star must be the secondary in the HE0532–4503 binary system, and since it did not explode in a supernova, we assumed it spun up the pulsar. As we were expecting to find an MSP (see, e.g., Wu et al. 2018), the period of the newly-found pulsar was somewhat long, at 157.28 ms. Perhaps the second stage of mass transfer was interrupted relatively quickly for the common-envelope stage? The sdB-PSR association hypothesis was furthermore challenged by the absence of measurable acceleration in the initial 2.1-hr observation, a significant fraction of the 6.5-hr orbit. Perhaps the sdB star was lighter than expected? We aimed to quickly confirm the pulsar and localise it through timing to answer these questions.

Under director’s discretionary time, we observed the system five more times with GBT and we obtained several observations with uGMRT. An overview of the follow-up observations is given in Table 2. The table also shows the S/N of the detected periodic signal when detected, as well as the number of detected single pulses.

The periodic signal was detected in three out of six GBT observations, confirming that the candidate is indeed a real pulsar. We next aimed to localise the pulsar to determine whether or not it could be part of the sdB binary system.

5.1 Localisation

The pulsar was observed on four consecutive days in May 2018 with GBT, spread out evenly over the sdB orbit to cover all orbital phases with the aim to detect the acceleration of the pulsar in its expected orbit around the sdB and to start a timing solution to localise it precisely. Interestingly, the pulsar was detected in only one of these

³ GBT observer guide <https://science.nrao.edu/facilities/gbt/observing/GBTog.pdf>

Table 2. Overview of observations of PSR J0533–4524. For completeness, we list not only the follow-up observations but also the original discovery observation taken on 20111018. For GBT observations, we used GUPPI at 300–400 MHz. With uGMRT, we used GWB at 300–500 MHz, and we recorded coherently and incoherently beamformed data, as well as interferometric data. The periodic flux density was determined using the radiometer equation, with the sensitivity scaled to the position of the pulsar (see Sect. 5.1) in the beam. We assume 20% errors on these flux densities. The number of single pulses above $S/N = 8$ are listed in the 6th column. Finally, we indicate the orbital phase of HE0532–4503, assuming an orbit of 0.2656 ± 0.0001 d (Geier et al. 2010), at the mid-point of the observation, relative to the 20160528 GBT observation. We only list these for epochs spaced closely enough in time to have an error on the orbital phase of less than 0.05. In addition to the observations listed here, we obtained one observation with Parkes, but as described in Sect. 5.1, it had no significant sensitivity in the direction of the pulsar so we did not consider it further.

Date	MJD	Telescope	t_{obs} (hr)	S/N	Periodic average flux density (mJy)	Number of single pulses	Relative orbital phase (0.0–1.0)
20111018	55852.3417	GBT	2.1	22	1.02(20)	3	
20160528	57536.76	GBT	1.6	<6	<0.32(6)	0	0.0
20160529	57537.75	GBT	1.5	<6	<0.32(6)	2	0.76
20160530	57538.75	GBT	1.5	<6	<0.33(7)	4	0.50
20160531	57539.75	GBT	1.5	7	0.37(7)	4	0.26
20160805	57605.56	GBT	1.6	11	0.55(11)	5	
20161106	57697.80	uGMRT	4.5	19, 7 ^(a)	0.44(9)	11	
20170108	57761.65	uGMRT	3.9	<6	<0.16(3)	0	
20170302	57814.57	uGMRT	2.2	<6	<0.20(4)	0	
20181103	58424.93	uGMRT	1.6	<6	<0.20(4)	0	
20181201	58452.78	uGMRT	1.9	<6	<0.18(4)	0	
20190103	58486.66	uGMRT	1.1	<6	<0.24(5)	0	
20190201	58515.67	uGMRT	1.7	50 ^(b)	0.58(10)	120	
20190301	58543.50	uGMRT	1.7	<6	<0.05(1)	6	

- (a) in the incoherently and coherently beamformed data, respectively.
 (b) in the coherently beamformed data.

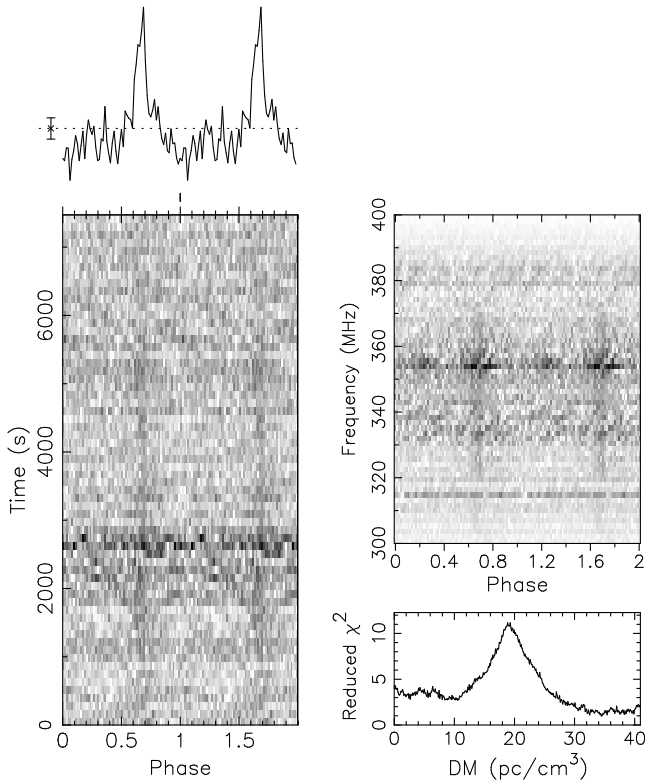


Figure 1. Discovery of PSR J0533–4524 with GBT. The signal is strongly peaked (top-left, two rotational periods shown), detected in the first 1.7 hrs out of the 2.1-hr observation (bottom-left) and broadband (top-right), with a well-defined dispersion measure (bottom-right).

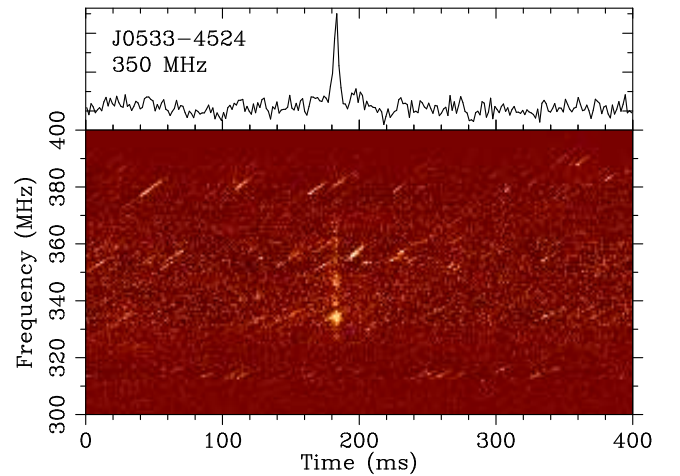


Figure 2. Brightest PSR J0533–4524 giant pulse detected with GBT, with a peak flux density of 3.7 Jy and fluence of 19 Jy-ms.

four observations. In the detection data, there was, again, no hint of acceleration. By itself this does not *rule out* the association: The binary could also be more face-on than assumed from the optical radial velocity curves, or the difference in mass between the two binary companions may have been larger than assumed. But the opposite, a detection of the acceleration, could have immediately associated the pulsar firmly with the sdB star. Due to the high fraction of non-detections, there were not enough data points to localise the pulsar through timing, either. We ruled out a number of reasons for the non-detections: the RFI situation between the four were similar and the test pulsar was detected equally well in all, indicating our sensitivity in all four was the same (Table 1); the orbital phases between the four were significantly different, ruling

out that eclipses play a major role; and we searched in period, period derivative, and dispersion measure. After eliminating these causes, the most probable remaining reason for the non-detections was intrinsic nulling or moding behaviour in the pulsar.

We then proceeded to observe the pulsar with uGMRT using several observing modes simultaneously. Beamformed data were recorded using both an incoherent addition of typically 16 dishes, as well as a coherent addition of the central 12 antennas. The incoherent mode retains the half-power beam width of a single uGMRT dish, $\sim 70'$, which covers the full field as observed with GBT. The coherent mode has a half-power beam width of $\sim 5'$, but is a factor three more sensitive than the incoherent mode. Since the sdB system was used as the pointing centre, the pulsar would be in the centre of the beam if it were part of the sdB system, and hence have a higher S/N in the coherent data than in the incoherent data. The pulsar was indeed detected, however the S/N was three times higher in the *incoherently* beam-formed data. The test pulsar did have a higher S/N in the coherent data, so the system performed as expected. Hence, we conclude that the pulsar is not associated with the sdB binary system.

In addition to beamformed data, interferometric data were recorded. Using the hypothesised nulling behaviour of the pulsar to our advantage, we aimed to image the field of both an observation with a detection and non-detection of the pulsar in beamformed mode. Any source in the image that shows the same on/off behaviour and has a flux density consistent with the flux density measured in beamformed data, might be the pulsar. The image created from the 20161106 uGMRT observation contained the pulsar in its on state (Fig. 3).

An off-state image was made from the data taken on 20181103. We identified one source, at RA = 05:33:14, Dec = $-45:24:50$, that was only present in the on-state image. The detection and non-detection images are shown in Fig. 3. This refined position was used for the last two uGMRT follow-up observations on 20190201 and 20190301.

In the 20190201 observation, the pulsar signal was clearly detected with an integrated S/N of 50 and corresponding average flux density of 0.58(10) mJy, which was the most significant detection thus far. In addition, over 100 single pulses were detected. We are thus confident that the source identified in the image is indeed the pulsar. Due to issues with processing of the interferometric data, the images created from the 20190201 and 20190301 observations did not have enough sensitivity to be able to identify the pulsar. The pulsar position is $\sim 20'$ from the sdB position and localised to $< 1'$, hence we conclude the pulsar and sdB are not associated.

The pulsar was also observed with Parkes in April of 2016 for 6.7 hrs but no periodic signal nor single pulses were found. As the half-power beam radius is $< 8'$ for Parkes' H-OH receiver at 1.4 GHz, the observation had little sensitivity towards the pulsar position, giving an upper limit of 45(9) mJy⁴. Given also the unknown pulsar spectral index, the non-detection is not surprising. We therefore did not consider this observation further.

5.2 Giant pulse emission

There are several definitions of giant pulses, but a broadly accepted one is any pulse that has a period-averaged flux density that is at least

ten times higher than the mean flux density of the periodic signal (Johnston & Romani 2004; Cairns 2004; Karuppusamy et al. 2010; Singal & Vats 2012; Maan et al. 2019). They are also narrower than the integrated profile and sometimes occur in a very narrow phase window (Knight 2006). To classify single pulses from J0533–4524, we considered the 20190201 uGMRT observation, which is the only observation with a periodic detection and the source in the centre of the beam.

The S/N of individual pulses reported by the `SINGLE_PULSE_SEARCH.PY` tool from PRESTO already correspond to a downsampling in time which maximises their S/N . This is equivalent to defining the width as the width of a top-hat with the same peak and integrated S/N as the observed pulse. We use this downsampling factor as an approximation for the actual pulse-width. The sky background temperature towards the source is estimated to be 17 K (Haslam et al. 1982). We have assumed T_{rec} to be 125 K, implying a total T_{sys} of 142 K (the observatory specifies a T_{sys} range of 100–165). We used these parameters in the modified radiometer equation to compute the peak flux density (Cordes & McLaughlin 2003; Maan & Aswathappa 2014) of individual pulses.

To compare the derived peak flux densities to the flux density of the periodic signal we define the period-averaged flux density of a single pulse as $\bar{S}_p = S_p \times W/P$, where S_p is the peak flux density, W is the width of the single pulse and P is the period of the pulsar. \bar{S}_p incorporates any differences in width between the periodic profile and single pulses, which makes it the appropriate parameter for comparison between single pulses and the periodic signal. The cumulative distribution function (CDF) of detected single pulses is shown in Fig. 4. The giant pulse threshold of ten times the mean flux density of 0.58 mJy (cf. Table 2) is shown as dashed green line. 92% of the detected single pulses are above this threshold. Hence they are consistent with being giant pulses.

Even assuming we are complete down to a S/N of 8, the completeness in S_p depends on the pulse width. If the widest observed pulse were detected at $S/N = 8$, it would have a peak flux density of 7.5 mJy. We take this value as our completeness threshold. The slope of the best-fit power law to the pulses above the completeness threshold is $-3.68(1)$.

Using the barycentric period measured in the 20190201 observation with `PREPFOLD` from PRESTO, the barycentric arrival time of each of the 120 single pulses was converted to a rotational phase. A histogram of the resulting phases is shown in Fig. 5, with the integrated profile shown for reference. All pulses occur within a phase window of 0.04, where the peak matches that of the integrated profile. They do not occur in the trailing component of the integrated profile. The giant pulses have widths between 2.5 and 10.0 ms, which is 10-30% of the width of the integrated profile (24 ms), where the width is defined as the width of a top-hat with the same peak value and integrated flux density as the observed pulse. These widths are a similar fraction of the mean pulse as the giant pulses observed in PSR B0950+08 Tsai et al. (2015). Together with the narrow phase window centred on one component of the integrated profile, this supports that the single pulses are indeed giant pulses (Knight 2006).

5.3 Nulling and mode changing

The initial seemingly erratic series of detections and non-detections (see Table 2) were reminiscent of the struggle to confirm and study mode-changing, nulling, and intermittent pulsars as PSRs B1931+24 (Kramer et al. 2006), B0826–34 (van Leeuwen & Timokhin 2012), and J1929+135 (Lyne et al. 2017).

⁴ Using $G = 0.83 \text{ K/Jy}$ and $T_{\text{rec}} = 25 \text{ K}$ from the Parkes user guide (https://www.parkes.atnf.csiro.au/observing/documentation/user_guide/pks_ug_3.html)

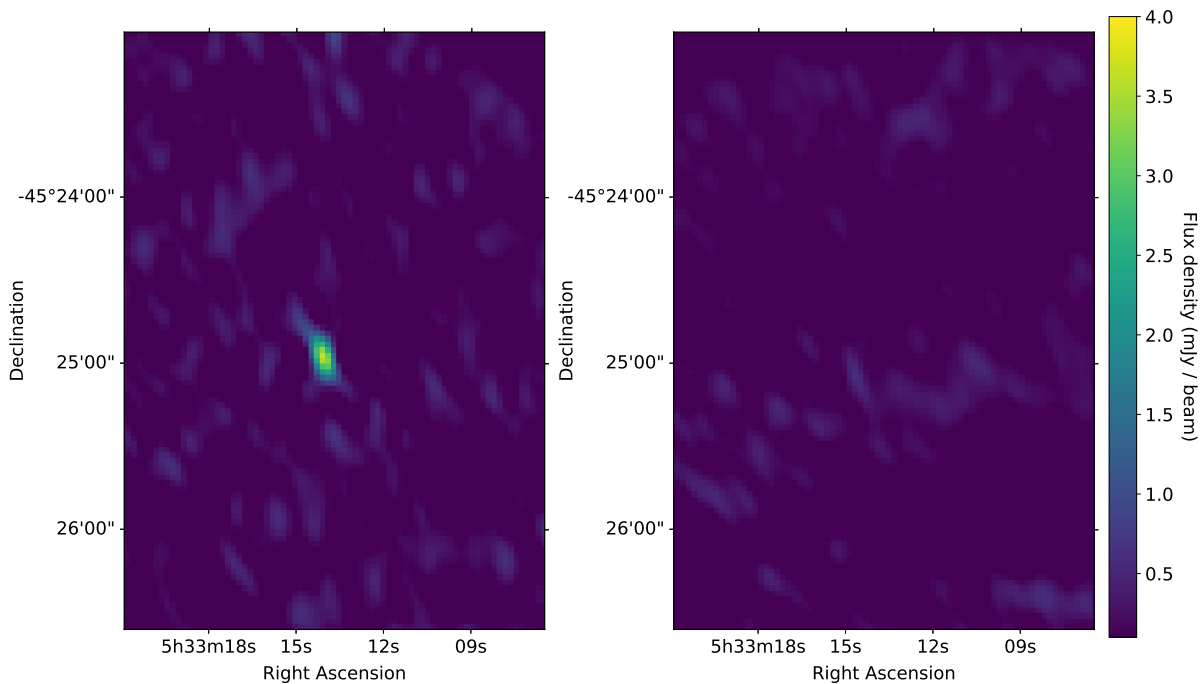


Figure 3. uGMRT images from observing sessions with detection on 20161106 (left) and non-detection on 20181103 (right) of the pulsar in beamformed mode. The source shown here is the only source of which the flux density in the image correlates with the flux density of the pulsar in beamformed mode, hence we assume it is in fact the pulsar.

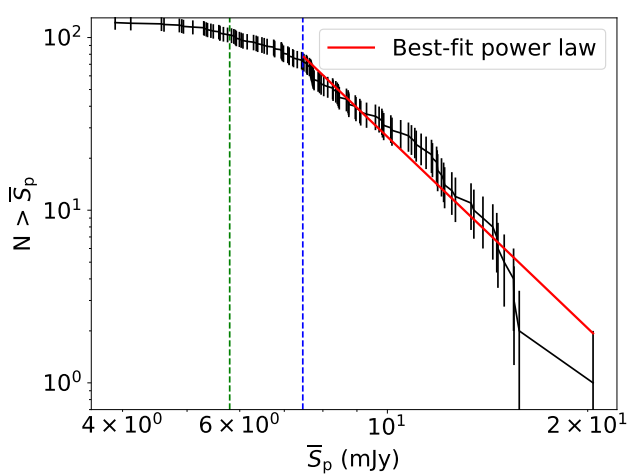


Figure 4. Cumulative distribution of period-averaged flux density of detected single pulses in log-log space. The vertical dashed lines indicate the giant pulse threshold of 10 times the mean flux density (5.8 mJy, green) and completeness threshold (7.5 mJy, blue). The best-fit power law for all pulses above the completeness threshold (red) has a slope of $-3.68(1)$.

The disappearance of the source near the end of the discovery observation (see Fig. 1) suggests that its flux density decreased, but it was observed very close to the horizon and might have set instead. Part of the variation in observed flux density in different observations is due to the initial positional uncertainty, and mis-pointing. But sets of detections using similar telescope setups can be compared among themselves, to analyse if intrinsic mode changing is also at play. In Fig. 6 we visualise the period and single-pulse

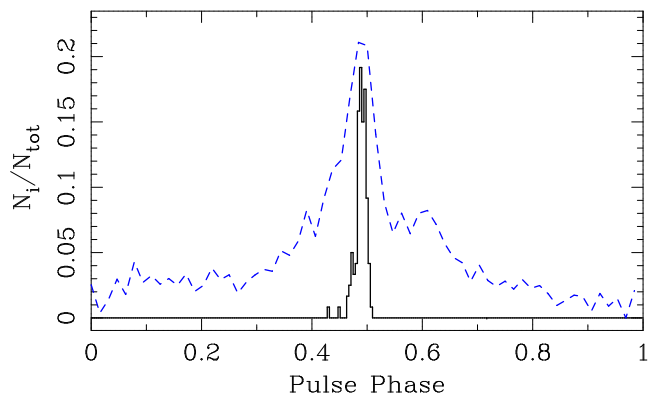


Figure 5. Distribution of rotational phase of single pulses (black) overlaid on the integrated pulse profile (blue). The giant pulse occur in a very narrow phase window around the peak of the integrated profile. They do not occur in the trailing edge component of the integrated profile.

detections. Sets demarcated by dashed lines were observed with the same setup and can be meaningfully compared.

We see that the periodic average flux density for observations *with* detections is only a factor of a few above our upper limits for non-detections. The fact that the initial detection is brighter than average can be explained by a discovery bias. Only in the last epoch, using the coherent uGMRT at boresight, there is a factor of 10 difference between the periodic average flux density and non-detection upper limit. In known nulling and mode-changing pulsars such as B0809+74 (van Leeuwen et al. 2002) and B0826–34, the flux density at the source changes by a factor of order 50 (Esamdin et al. 2005).

In the first set of observations, the giant-pulse occurrence rate

and peak flux density do not appear to correlate with whether periodic emission is detected. In the second set, they do. There, each observation either delivered the detection of both periodic and giant-pulse emission, or of neither.

Overall, the difference between our detections and upper limits does not reach the brightness difference of several orders of magnitude generally seen in nulls or between modes. We thus conclude our data *suggest* nulling, but are not constraining enough to *prove* nulling or mode changing.

5.4 Timing

In order to characterise the pulsar parameters, we aimed to create a coherent timing solution. For several observations, only single pulses are detected. As the single pulses occur in a very narrow phase window around the peak of the integrated pulse, both the single pulse and periodic arrival times can be used to form a timing solution. For both the periodic profile and single pulses a template profile was created using `DSPSR` and `PSRCHIVE`, based on the highest S/N detections. Times-of-arrival (TOAs) were then extracted from each single pulse, as well as from each periodic detection. For both single pulse and the periodic signal we used a pulse profile template with the same phase and shape, but with a different width determined from the highest S/N data. For observations where the periodic S/N was high enough, the observation was split into chunks of at least S/N 8 each and TOAs were extracted for each chunk.

We then proceeded timing with `TEMPO2`. When the position was updated to the variable source discovered in the imaging data, it was possible to find a coherent solution for the 2016 – 2019 data. The 2011 points then also fit the solution well, so they were included in the analysis. Then, the DM was fit by splitting the highest S/N periodic detection into 32 frequency chunks and fitting with `TEMPO2`. Finally, the position was then allowed to vary as well. The final derived position is consistent with that measured from the imaging technique. The fit parameters are shown in Table 3.

The DM suggests a distance of 0.7 kpc using the NE2001 electron model (Cordes & Lazio 2002) and 1.3 kpc using YMW16 (Yao et al. 2017). The obtained period of 157.28 ms and \dot{P} of 2.8×10^{-16} suggest a characteristic age (defined as $P/2\dot{P}$) of ~ 10 Myr and surface magnetic field (defined as $10^{12}\sqrt{P\dot{P}}$ G, with P in seconds) of $\sim 2 \times 10^{11}$ G. The pulsar is thus a bit older than one might expect given its period, but it has a relatively low magnetic field. These parameters are similar to PSR B0950+08, which has a period of 253 ms, and period derivative of 2.3×10^{-16} (Hobbs et al. 2004).

6 DISCUSSION

In Sect. 4 we have shown that given the derived beaming fraction of known MSPs, and their place in the luminosity distribution, at most three out of six systems can be expected to be millisecond radio pulsars. Furthermore, all three would be beamed away from us or too dim to be detected. It might also be possible that the pulsars are only mildly recycled, and their beams have a significant chance to miss Earth. In both cases we cannot exclude that they are all neutron stars, just not detectable in radio.

To establish whether it is reasonable to assume all six systems host a neutron star, we consider two aspects: the neutron star birth rate and their behaviour in binary systems.

Supernova modelling already indicates a lower rate of neutron-star formation than appears to be required to produce the number of pulsars observed (cf. Keane & Kramer 2008). Is this problem twice

Table 3. Parameters of the best-fit timing solution determined with `TEMPO2`.

<i>Fit and data-set</i>	
Pulsar name	PSR J0533–4524
MJD range	55852 – 58544
Weighted RMS timing residual ^(a) (μ s)	1105.453
χ^2_{red}	6.0
<i>Set quantities</i>	
Period epoch (MJD)	57605.55728
<i>Measured quantities</i>	
DM (pc cm ⁻³)	18.93(2)
RA	05:33:13.89(4)
Dec	-45:24:50.2(2)
P (s)	0.157284525096(2)
\dot{P} (s/s)	$2.8024(2) \times 10^{-16}$
<i>Derived quantities</i>	
Characteristic age (Myr)	8.8925(4)
B_{surf} (G)	$2.1245(1) \times 10^{11}$

^(a) Defined as the root-mean-square deviation from zero of each residual, weighted by its uncertainty.

as bad, if half of neutron stars are not detectable as radio pulsars, as our observations seem to suggest? Not directly. The neutron-star birth rate for successful modelling of the Galactic population, in such population synthesis as Faucher-Giguère & Kaspi (2006) and van Leeuwen & Stappers (2010), is only that of regular, non-recycled pulsars. These first shine during their regular lives, to then possibly be reborn as MSPs. Systems that will later evolve into systems like our six may currently be visible as regular pulsars, where they are properly counted toward the neutron-star birth-rate problem. The closest such system, i.e., a currently observed pulsar that may later evolve into an sdB-PSR binary, is PSR J0045–7319 (Kaspi et al. 1994), and there are two similar but more massive known binaries.

The Small Magellanic Cloud pulsar PSR J0045–7319 has a companion of type B1 V, of 8–10 M_{\odot} (Kaspi et al. 1994). The pulsar there is not yet recycled and the orbit is still 51 days. For a B-type companion of such $>5 M_{\odot}$ mass Wu et al. (2018) predict common envelope evolution, with short (\sim hour) orbits, similar to the six candidate systems investigated in this work (Table 1).

The binary companion to PSR B1259–63 (Johnston et al. 1992) is now thought to have a mass of 15–31 M_{\odot} (Miller-Jones et al. 2018), which may be too large to become an sdB star. While it was thought to be a Be star for the first few years after its discovery, it is currently classified as Oe star. Similarly, the latest timing on PSR J1740–3052 indicates its companion has a mass of 16–26 M_{\odot} (Madsen et al. 2012), and the most likely optical counterpart is a main sequence star of late O or early B type (Bassa et al. 2011).

Together, these three observed systems qualitatively suggest our non-detections do not immediately create a birth-rate problem. Is the recycling process perhaps not reliable?

In the previous discussion we have estimated the beaming fraction f_b , the odds that the beam of an active MSP sweeps across Earth. But what is the fraction f_r of systems that is successfully recycled? As the beaming fraction allows for 3 of 6 systems to go unseen, we conclude an additional factor $f_r < 0.5$ must be needed to explain our non-detections. Such a fraction significantly smaller than 1 is in line with the number of radio non-detections in other systems where neutron stars could viably be present as pulsars. These targeted searches included binaries such as low-mass white

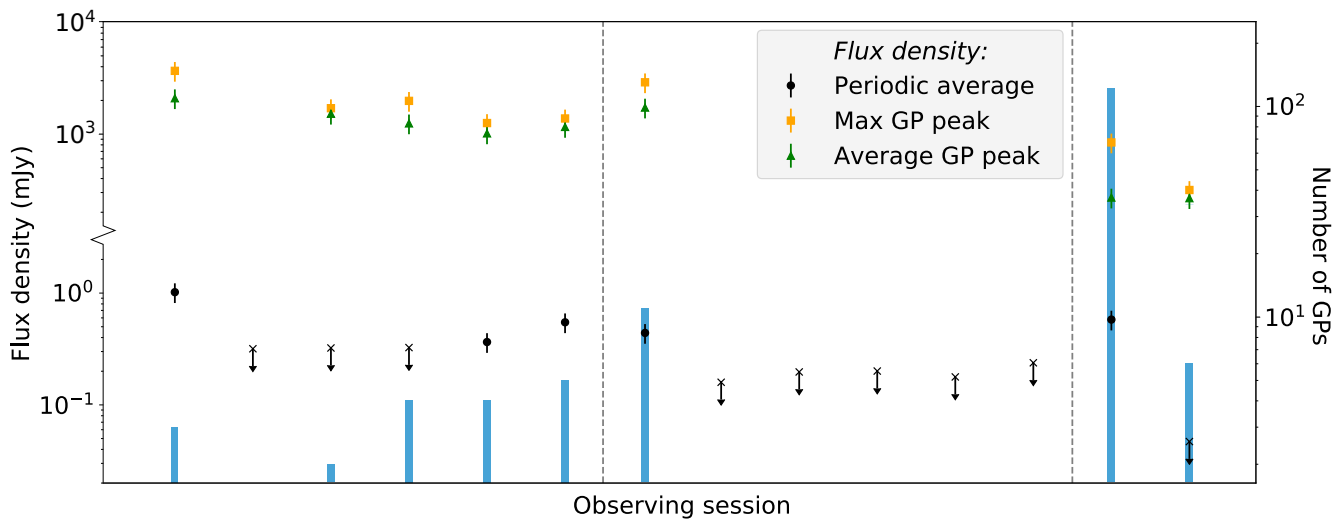


Figure 6. Overview of periodic and single pulse behaviour in PSR J0533–4524. The periodic average flux density is shown as black dots, with upper limits shown as crosses. The average and brightest giant pulse flux density are shown in green and orange, respectively. Error bars indicate 1σ errors. A histogram of the number of detected giant pulses in each session is shown in blue. The vertical dashed lines indicate changes to a different observing setup: The first six sessions were with GBT, sessions seven through twelve are based on uGMRT in incoherent mode, all with the pulsar not at boresight. The last two sessions were with uGMRT in coherent mode, with the pulsar at boresight.

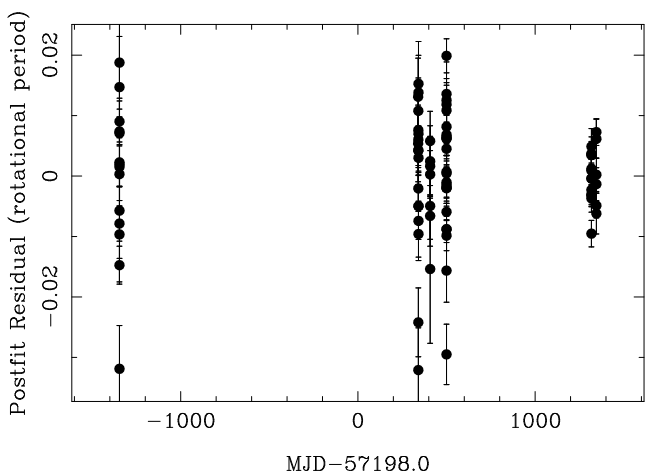


Figure 7. Timing residuals of PSR J0533–4524. We obtained 82 (25 periodic and 57 single-pulse) arrival times spread over ~ 7 years. The mean residual is $< 1\%$ of the pulse period. See also Table 3

dwarfs (van Leeuwen et al. 2007; Agüeros et al. 2009), OB runaway stars (Sayer et al. 1996), and soft X-ray transients (Mikhailov et al. 2017). Even the radio detection of PSR J1417–4402 by Camilo et al. (2016) appears to have occurred independently from the optical identification of the binary 1FGL J1417.7–4407 (Strader et al. 2015).

It remains possible that all observed sdB binaries in fact host a neutron star, but all of them would either be beamed away from Earth, too dim, or not recycled. Could it be possible that some systems actually host a white dwarf instead of a neutron star? This would mean that their masses must be below $1.4M_{\odot}$. The masses are determined under the assumption of co-rotation, so the orbital period of the system is assumed to be equal to the rotation period of the sdB. This allows for determination of the inclination angle and hence the mass ratio of the two components. As the range of

masses allowed for sdB stars is quite small, this gives the mass of the secondary to reasonable precision. If some of the suspected neutron stars are actually white dwarfs, their masses must have been overestimated. Getting to the right mass range would require either the sdB mass to be much smaller, which seems nonphysical, or the derived inclination angle to be too high, which could happen if the assumption of co-rotation breaks down. If these systems are actually more edge on, the predicted masses would be lower. This would also solve the inclination problem posed by Geier et al. (2010). We note that for a random distribution of inclination angles, the most probable value is 52° , which puts the predicted secondary masses in the $0.9\text{--}1.0M_{\odot}$ range. It therefore seems likely that several of the observed sdB system actually host white dwarfs if the assumption of co-rotation does not hold. Only PG 1232–136 still has a predicted mass of $>1.4M_{\odot}$ and remains a viable system to host either a neutron star or black hole.

X-ray emission may be expected from sdB-NS systems due to thermal emission of the neutron star or accretion of the sdB wind (Mereghetti et al. 2011). However, targeted searches for X-ray emission from our six targets have not yielded any detections (Mereghetti et al. 2011, 2014). This further suggests the absence of neutron stars although it might also be explained by mass-loss rates that are lower than predicted by theoretical models. These non-detections also confirm that there is no significant accretion due to Roche-Lobe overflow, which is expected given that sDBs are much smaller than their Roche Lobe.

6.1 PSR J0533–4524

6.1.1 Is PSR J0533–4524 an RRAT

We observe pulsar J0533–4524 often emits strong individual pulses. Should it then be classified as a rotating radio transient (RRAT)? According to the definition proposed in McLaughlin et al. (2006), one of the characteristics of an RRAT is that its period is determined from the single pulses, and cannot be derived from periodic emission. Initial observations fit this definition. But, as we were

able to measure the period from the Fourier search on the 20111018 observation, J0533–4524 is ultimately not an RRAT.

6.1.2 Giant pulse emission revisited

While the single pulses detected from J0533–4524 are giant pulses according to the typical definition, we consider they might be the bright end of a single underlying single-pulse distribution, as was determined for PSR B0950+08 (Tsai et al. 2016). While for B0950+08, the underlying distribution is assumed to be Gaussian, Kramer et al. (2002) showed that several pulsars have a log-normal pulse brightness distribution.

Assuming J0533–4524 has a log-normal distribution of single pulses, we can predict the slope of the observed CDF of single pulses without fully knowing the underlying single-pulse distribution. The fraction of detectable single pulses, f_{sp} , is equal to the chance of detecting a pulse that is more than $n\sigma$ brighter than the mean pulse (μ) for some unknown n , and is given by the complement of the CDF of the log-normal distribution,

$$f_{\text{sp}} = \frac{1}{2} \operatorname{erfc}\left(\frac{n}{\sqrt{2}}\right), \quad (4)$$

where erfc is the complementary error function.

The slope of the CDF of detected single pulses is then given by the derivative of Eq. 4. Rewriting in terms of f_{sp} gives

$$\frac{\partial \log f_{\text{sp}}}{\partial \log n} = \frac{-\operatorname{erfc}^{-1}(2f_{\text{sp}})}{f_{\text{sp}}\sqrt{\pi}} \exp\left(-\operatorname{erfc}^{-1}(2f_{\text{sp}})^2\right), \quad (5)$$

where erfc^{-1} is the inverse of the complementary error function. The slope predicted by this equation is equal to the slope of the observed CDF if the distribution of the parameter that is chosen to create the CDF has a mean of zero. Evidently, this is not the case if the chosen parameter is the period-averaged flux density of the single pulses, \bar{S}_p . Instead, we choose $\log_{10}(\bar{S}_p/S_{p,\text{mean}})$, where $S_{p,\text{mean}}$ is the mean flux density of the periodic profile (0.58 mJy, see Table 2). The mean of the distribution then is equal to zero if there is indeed one underlying single-pulse distribution.

The observed distribution of $\log_{10}(\bar{S}_p/S_{p,\text{mean}})$ is shown in Fig. 8. 1σ error bars are shown assuming Poissonian errors. There are 72 single pulse above the completeness threshold defined in Sect. 5.2. In total, the pulsar has 3.8×10^4 turns in the 1.7-hr part of the observation where it was visible, implying $f_{\text{sp}} = 1.9 \times 10^{-3}$, which corresponds to detecting all single pulses that are at least 2.9σ brighter than the mean pulse. This also implies that the standard deviation of the underlying distribution is ~ 0.38 in units of $\log_{10}(\bar{S}_p/S_{p,\text{mean}})$.

Equation 5 then predicts a slope of -9.2 for the CDF of detected single pulses at the completeness threshold. Extrapolating from this point, the predicted CDF is shown in blue. It has a mean slope of -11 . The best-fit power law is shown in red and has a slope of $-10.6(4)$. The observed distribution is consistent with being the bright-end tail of a log-normal distribution of single pulses.

It is thus not straightforward to classify single pulses. In some cases, giant pulses may simply be the bright end of the distribution of normal pulses. However, their width and phase are different from those of the average pulse and when averaged together they do not recover the periodic integrated profile. More research into this subject is needed to determine whether this means the J0533–4524 giant pulses are actually from a different distribution than the normal pulses, or whether it implies a correlation between these parameters

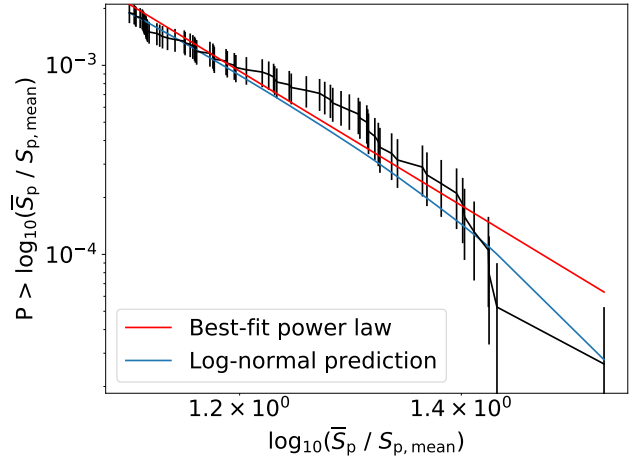


Figure 8. Cumulative distribution of $\log_{10}(\bar{S}_p/S_{p,\text{mean}})$ of detected single pulses. The best-fit power law is shown. The slope is $-10.6(4)$ in log-log space, which is consistent with the value predicted for the tail of a log-normal distribution of single pulses (-11).

and pulse brightness. A correlation between pulse width and brightness is seen in for example the Crab giant pulses (Karuppusamy et al. 2010), where narrower pulses are typically brighter.

If giant pulses are simply the tail of the normal single-pulse distribution, then why are they not detected in all pulsars given enough observation time? This may be due to differences in the width of the normal pulse distribution. For J0533–4524, a pulse that is 3σ above the mean is roughly ten times brighter than the mean pulse, and hence classified as a giant pulse. If, however, the single-pulse distribution were narrower, a pulse with ten times the mean flux density would be much more rare. For example, the single-pulse distribution of a standard pulsar such as PSR B0818–13 in its on state (Janssen & van Leeuwen 2004) has virtually no pulses that are more than twice as bright as the mean. Perhaps several giant-pulse emitting pulsars are classified as such because they have a relatively broad single-pulse distribution, such that it is feasible to detect pulses over ten times the mean within a typical observation length.

7 CONCLUSIONS

We searched for radio pulsations from six sdB binary systems that are likely to host a neutron star based on sdB orbital parameters derived from optical observations. No pulsars were detected towards sdB systems down to an average flux density limit of 0.13 mJy at 350 MHz. For the systems also presented in Coenen et al. (2011), the upper limits are a factor 2-3 deeper. The non-detection of any pulsar towards the sdB binary systems could be explained by a combination of the putative MSP beaming fraction, luminosity, and a recycling fraction $f_r < 0.5$. If some of the sdBs systems do host a pulsar, the most likely reason for non-detection is that their beams do not sweep across the Earth. Therefore it is unlikely that deeper searches, either through longer observations or through the use of more sensitive telescopes, such as Arecibo and FAST, will be fruitful. However, it is possible that there might be a pulsar with extremely faint emission, which may be detectable with the aforementioned instruments. It is also possible that the assumption of co-rotation of the sdB in its orbit does not hold, in which case the masses of the sdB companions

are likely over-predicted. Then, several systems could host a white dwarf instead of a neutron star.

We discovered PSR J0533–4524, a giant-pulse emitting pulsar. Through simultaneous beamformed and interferometric observations with uGMRT, the pulsar was localised and shown to be a serendipitous discovery, not associated with the sdB system that was the original target. We detected over 100 giant pulses from this pulsar. Their distribution is compatible with the tail of a log-normal distribution with the same mean as the average single pulse, showing that we may be seeing the bright end of the normal single pulses. However, the giant pulses are narrower than the integrated pulse and restricted to a very narrow phase window, unlike what is expected from the average single pulses.

ACKNOWLEDGEMENTS

We thank J. Lazio for providing the data on HE 0929–0424 and PG 1232–136 and E. Petroff for observing HE 0532–4503 with Parkes. Additionally, we thank the anonymous referee for providing useful comments that helped improve the manuscript. LCO, JvL, and YM acknowledge funding from the European Research Council under the European Union’s Seventh Framework Programme (FP/2007–2013)/ERC Grant Agreement No. 617199. The Green Bank Observatory is a facility of the National Science Foundation operated under cooperative agreement by Associated Universities, Inc. The Westerbork Synthesis Radio Telescope is operated by ASTRON (The Netherlands Institute for Radio Astronomy) with support from the Netherlands Foundation for Scientific Research (NWO). GMRT is run by the National Centre for Radio Astrophysics of the Tata Institute of Fundamental Research.

References

- Agüeros M. A., Camilo F., Silvestri N. M., Kleinman S. J., Anderson S. F., Liebert J. W., 2009, *ApJ*, **697**, 283
- Alpar M. A., Cheng A. F., Ruderman M. A., Shaham J., 1982, *Nature*, **300**, 728
- Bagchi M., Lorimer D. R., Chennamangalam J., 2011, *MNRAS*, **418**, 477
- Bassa C. G., Brisken W. F., Nelemans G., Stairs I. H., Stappers B. W., Kramer M., 2011, *MNRAS*, **412**, L63
- Bates S. D., et al., 2015, *MNRAS*, **446**, 4019
- Cairns I. H., 2004, *ApJ*, **610**, 948
- Camilo F., et al., 2015, *ApJ*, **810**, 85
- Camilo F., et al., 2016, *ApJ*, **820**, 6
- Chen X., Han Z., Deca J., Podsiadlowski P., 2013, *MNRAS*, **434**, 186
- Coenen T., van Leeuwen J., Stairs I. H., 2011, *A&A*, **531**, A125+
- Cognard I., Shrauner J. A., Taylor J. H., Thorsett S. E., 1996, *ApJ*, **457**, 81
- Cordes J. M., Lazio T. J. W., 2002, *ArXiv:astro-ph/0207156*,
- Cordes J. M., McLaughlin M. A., 2003, *ApJ*, **596**, 1142
- Dewey R. J., Taylor J. H., Weisberg J. M., Stokes G. H., 1985, *ApJ*, **294**, L25
- Drilling J. S., Jeffery C. S., Heber U., Moehler S., Napiwotzki R., 2013, *A&A*, **551**, A31
- Esamdin A., Lyne A. G., Graham-Smith F., Kramer M., Manchester R. N., Wu X., 2005, *MNRAS*, **356**, 59
- Faucher-Giguère C.-A., Kaspi V. M., 2006, *ApJ*, **643**, 332
- Freire P. C. C., et al., 2012, *MNRAS*, **423**, 3328
- Gaia Collaboration et al., 2018, *A&A*, **616**, A1
- Geier S., Heber U., Podsiadlowski P., Edelmann H., Napiwotzki R., Kupfer T., Müller S., 2010, *A&A*, **519**, A25
- Geier S., Østensen R. H., Nemeth P., Gentile Fusillo N. P., Gänsicke B. T., Teltng J. H., Green E. M., Schaffnerroth J., 2017, *A&A*, **600**, A50
- Gupta Y., et al., 2017, *Current Science*, **113**, 707
- Han Z., Podsiadlowski P., Maxted P. F. L., Marsh T. R., Ivanova N., 2002, *MNRAS*, **336**, 449
- Han Z., Podsiadlowski P., Maxted P. F. L., Marsh T. R., 2003, *MNRAS*, **341**, 669
- Haslam C. G. T., Stoffel H., Salter C. J., Wilson W. E., 1982, *A&AS*, **47**, 1
- Heber U., 1986, *A&A*, **155**, 33
- Heber U., 2016, *PASP*, **128**, 082001
- Hobbs G. B., Manchester R. N., 2004, *ATNF Pulsar Catalogue*, <http://www.atnf.csiro.au/research/pulsar/psrcat/>
- Hobbs G., Lyne A. G., Kramer M., Martin C. E., Jordan C., 2004, *MNRAS*, **353**, 1311
- Jaffe A. H., Backer D. C., 2003, *ApJ*, **583**, 616
- Janssen G. H., van Leeuwen J., 2004, *A&A*, **425**, 255
- Johnston S., Romani R. W., 2004, in *IAU Symposium No. 218: Young neutron stars and their environments*. pp 315–318
- Johnston S., Manchester R. N., Lyne A. G., Bailes M., Kaspi V. M., Qiao G., D’Amico N., 1992, *ApJ*, **387**, L37
- Karuppusamy R., Stappers B. W., van Straten W., 2010, *A&A*, **515**, A36
- Kaspi V. M., Johnston S., Bell J. F., Manchester R. N., Bailes M., Bessell M., Lyne A. G., D’Amico N., 1994, *ApJ*, **423**, L43
- Keane E. F., Kramer M., 2008, *MNRAS*, **391**, 2009
- Knight H. S., 2006, *Chinese Journal of Astronomy and Astrophysics Supplement*, **6**, 41
- Kramer M., Xilouris K. M., Lorimer D. R., Doroshenko O., Jessner A., Wielebinski R., Wolszczan A., Camilo F., 1998, *ApJ*, **501**, 270
- Kramer M., Johnston S., van Straten W., 2002, *MNRAS*, **334**, 523
- Kramer M., Lyne A. G., O’Brien J. T., Jordan C. A., Lorimer D. R., 2006, *Science*, **312**, 549
- Lattimer J. M., Prakash M., 2001, *ApJ*, **550**, 426
- Lawson K. D., Mayer C. J., Osborne J. L., Parkinson M. L., 1987, *MNRAS*
- Lorimer D. R., Kramer M., 2005, *Handbook of Pulsar Astronomy*. Cambridge University Press
- Lyne A. G., et al., 2017, *ApJ*, **834**, 72
- Maan Y., Aswathappa H. A., 2014, *MNRAS*, **445**, 3221
- Maan Y., Bassa C., van Leeuwen J., Krishnakumar M. A., Joshi B. C., 2018, *ApJ*, **864**, 16
- Maan Y., Joshi B. C., Surnis M. P., Bagchi M., Manoharan P. K., 2019, *ApJ*, **882**, L9
- Madsen E. C., et al., 2012, *MNRAS*, **425**, 2378
- Manchester R. N., 2017, *Journal of Astrophysics and Astronomy*, **38**, 42
- Maxted P. F. L., Heber U., Marsh T. R., North R. C., 2001, *MNRAS*, **326**, 1391
- McLaughlin M. A., et al., 2006, *Nature*, **439**, 817
- Mereghetti S., Campana S., Esposito P., La Palombara N., Tiengo A., 2011, *A&A*, **536**, A69
- Mereghetti S., La Palombara N., Esposito P., Gastaldello F., Tiengo A., Heber U., Geier S., Wilms J., 2014, *MNRAS*, **441**, 2684
- Mikhailov K., van Leeuwen J., Jonker P. G., 2017, *ApJ*, **840**, 9
- Miller-Jones J. C. A., et al., 2018, *MNRAS*, **479**, 4849
- Nelemans G., 2010, *Ap&SS*, **329**, 25
- Parent E., et al., 2019, *ApJ*, **886**, 148
- Radhakrishnan V., Srinivasan G., 1982, *Curr. Sci.*, **51**, 1096
- Ransom S., 2011, *PRESTO: Pulsar Exploration and Search Toolkit* (ascl:1107.017)
- Rubio-Herrera E., Stappers B. W., Hessels J. W. T., Braun R., 2013, *MNRAS*, **428**, 2857
- Sanidas S., et al., 2019, *A&A*, **626**, A104
- Sayer R. W., Nice D. J., Kaspi V. M., 1996, *ApJ*, **461**, 357
- Singal A. K., Vats H. O., 2012, *AJ*, **144**, 155
- Strader J., et al., 2015, *ApJ*, **804**, L12
- Taylor J. H., Weisberg J. M., 1989, *ApJ*, **345**, 434
- Tsai J.-W., et al., 2015, *AJ*, **149**, 65
- Tsai Jr., Simonetti J. H., Akukwe B., Bear B., Gough J. D., Shawhan P., Kavic M., 2016, *AJ*, **151**, 28
- Webbink R. F., 1984, *ApJ*, **277**, 355
- Wu Y., Chen X., Li Z., Han Z., 2018, *A&A*, **618**, A14
- Yao J. M., Manchester R. N., Wang N., 2017, *ApJ*, **835**, 29
- Yungelson L. R., Tutukov A. V., 2005, *Astronomy Reports*, **49**, 871

- van Leeuwen J., Stappers B. W., 2010, [A&A](#), 509, 7
- van Leeuwen J., Timokhin A. N., 2012, [ApJ](#), 752, 155
- van Leeuwen J., Kouwenhoven M. L. A., Ramachandran R., Rankin J. M.,
Stappers B. W., 2002, [A&A](#), 387, 169
- van Leeuwen J., Ferdman R. D., Meyer S., Stairs I., 2007, [MNRAS](#), 374,
1437
- van Leeuwen J., et al., 2015, [ApJ](#), 798, 118